Magnetic properties of $R\mathrm{Fe}_{11.3}\mathrm{W}_{0.7}$ (R=Dy, Ho, Er, and Lu): On the R-Fe exchange interaction in the $R(\mathrm{Fe,T})_{12}$ class of compounds

N. Plugaru,* J. Rubín, J. Bartolomé, C. Piquer, and M. Artigas
Instituto de Ciencia de Materiales de Aragón-CSIC, Universidad de Zaragoza, 50009 Zaragoza, Spain
(Received 23 October 2001; revised manuscript received 14 January 2002; published 19 March 2002)

Results of x-ray powder diffraction and magnetic measurements performed on $R\mathrm{Fe}_{11.3}\mathrm{W}_{0.7}$ compounds, where R=Dy, Ho, Er, and Lu, are presented. The Curie temperature, saturation magnetization, and spin reorientation transitions are discussed in relation to several $R\mathrm{Fe}_{12-x}T_x$ systems, where T=Ta, Nb, Mo, Ti, and the x-substituent concentration is within a narrow range $x=0.5$–1.0. In these systems, the dependence of the Curie temperature versus the unit cell volume, for a given R partner, suggests combined size and electronic effects produced by the T atom. The strengths of the rare-earth–iron and iron-iron exchange interactions are evaluated in the mean-field framework, and analyzed with reference to $R\mathrm{Fe}_{12-x}T_x$ compounds, with T=Ta, Re, Nb, Mo, Ti, Cr, and V. Based on (i) the phenomenological mean-field model accounting for the sublattice of conduction band electrons, (ii) Brooks' reinterpretation of Campbell's formulation of the intersublattice exchange, and (iii) Wigner-Seitz cell analysis, we explore the role played by the conduction band electrons, particularly the nd-type electrons ($n=3$, 4, 5), on the intersublattice exchange coupling in the iron-rich $R\mathrm{Fe}_{12-x}T_x$ class of compounds. It is proposed that the variation in the conduction-electron density, by varying the T element type and concentration, leads to a modification of the $5d$ band occupancy number and consequently, of the R-Fe intersublattice exchange coupling.

DOI: 10.1103/PhysRevB.65.134419 PACS number(s): 75.30.Et, 75.30.Gw

I. INTRODUCTION

Recent investigations of $R\mathrm{Fe}_{12-x}T_x$ compounds, and their interstitial solid solutions with N, C, and H, were mainly carried on systems with a low content ($x\leqslant 1$) of the alloying element T, under the expectance of enhancing the technically useful hard magnetic properties. The interest in having as small an amount as possible of the third element, critical for the stabilization of the iron-rich phase with ThMn_{12}-type structure, S.G. $I4/mmm$, lies in the avoidance of the severe decrease in the Curie temperature and iron magnetization when increasing the T metal concentration to the upper limit of its solubility range.[1,2] However, up to the present only a few $R\mathrm{Fe}_{12-x}T_x$ systems are known which comply with this requirement; they form for T=Ta ($x\approx 0.5$–0.7),[3–6] Nb ($x\approx 0.6$–0.7),[7–12] Mo ($x\approx 0.5$–4.0),[13–15] and Ti ($x\approx 1$).[16] Apparently, the compounds with the highest iron content form when T is a $4d$ or $5d$ element, and particularly, with rare earths from Gd to Lu.

There are only a few reports on $R\mathrm{Fe}_{12-x}\mathrm{W}_x$ (see Ref. 2 and references cited therein). From the experimental point of view, they provide evidence of the formation of compounds with a ThMn_{12} structure for R=Gd and Y, with a W content in the range $1.2\leqslant x\leqslant 2$, when R=Sm, with $1.5\leqslant x\leqslant 2$ and R=Nd for $x=2$. Still, the limits of W solubility are not well established, and there is scarce information on their magnetic properties across the rare-earth series. There has been no report on $R\mathrm{Fe}_{12-x}\mathrm{W}_x$ compounds with smaller tungsten contents ($0.5\leqslant x\leqslant 1$). In theoretical studies, band-structure calculations were carried out only for the hypothetical, structurally ordered $\mathrm{YFe}_8\mathrm{W}_4$.[17] They predicted total and site-resolved magnetic moments in hypothetical YFe_8T_4 compounds, where T stands for the isoelectronic Mo and W atoms.

Previously, we studied, by x-ray diffraction, magnetic measurements,[3] and neutron diffraction,[4] the $R\mathrm{Fe}_{11.5}\mathrm{Ta}_{0.5}$ series of compounds. As a continuation of the systematic research on $R\mathrm{Fe}_{12-x}T_x$ phases stabilized with $5d$ elements, in this paper we present the structural and magnetic properties of the $R\mathrm{Fe}_{11.3}\mathrm{W}_{0.7}$ alloys. Particular interest is devoted to an analysis of the R-Fe exchange interactions in the $R\mathrm{Fe}_{12-x}T_x$ class of compounds as there were already experimental data reported on several systems with T being an nd-type element, where $n=3$, 4, and 5. Recently, the decisive role played by d states at R sites on the exchange interactions in R_xT_{1-x} intermetallics was reviewed.[18] In the present work we evaluate, in the mean field approximation, the strength of R-Fe exchange in the $R\mathrm{Fe}_{11.3}\mathrm{W}_{0.7}$ series, and analyze the results in relation to the data published for the corresponding compounds with T=Ta, Nb, Ti, and Re with $x\leqslant 1.2$, as well as T=Mo, V, and Cr with $x\geqslant 1.5$. Our approach highlights the major role played by the conduction band electrons, particularly the d electrons at R site on the intersublattice exchange coupling in $R\mathrm{Fe}_{12-x}T_x$ compounds. The discussion extends over several $R\mathrm{Fe}_{12-x}T_x$ series with R from Gd to Lu, since most of the systematic experimental data are reported for the compounds with the heavy-rare-earth (HRE) elements.

II. EXPERIMENT

The $R\mathrm{Fe}_{12-x}\mathrm{W}_x$ alloys investigated in the present study were prepared by melting pure elements (rare earths $3N$ purity, iron $3N7$, and tungsten $3N5$) in a high-frequency induction furnace, under an Ar atmosphere. In order to determine the range of compositions x for which the phase with the ThMn_{12} structure forms, several batches of $\mathrm{DyFe}_{12-x}\mathrm{W}_x$, with nominal stoichiometries $x=0.5$, 0.6, 0.7,

0.8, 1.0, 1.5, and 2.0, were cast. The choice of a HRE element for the trials was based primarily on the published experimental evidence which shows that $R\mathrm{Fe}_{12-x}T_x$, with T being a $4d$ or $5d$ element, forms systematically with the HRE,[1–15] and particularly Dy due to its lower cost among the HRE series. The ingots were checked for the phase content both in an as-cast form and annealed at 900 °C for one week. The identification of the phases and the structural study were performed by powder x-ray diffraction using a Siemens D501 diffractometer in the Bragg-Brentano geometry, with Cu-$K\alpha$ radiation, at room temperature. The diffraction patterns were Rietveld refined using the FULLPROF.98 Version 0.2 software.[19]

Thermomagnetic curves were measured with a Faraday-type balance between room temperature and 1073 K. The Curie temperature T_C was determined as the intersection point of the drop of magnetization part with the linear part of the curve at higher temperatures and the estimated error is ± 2 K.

We found that the majority phase with a $ThMn_{12}$ structure was formed in all $\mathrm{DyFe}_{12-x}\mathrm{W}_x$ samples. Also, different amounts of α-Fe and Dy_2Fe_{17} secondary phases were identified in samples with $0.5 \leqslant x \leqslant 1.0$, whereas WFe_2 was found in the alloys with $x=1.5$ and 2.0. The annealing significantly reduced the content in the 2:17 secondary phase. The least amounts of α-Fe and 2:17 secondary phases ($<10\%$, overall) were observed in annealed samples with x in the range 0.6–0.7.

Therefore, we prepared a $R\mathrm{Fe}_{11.3}\mathrm{W}_{0.7}$ series, with R = Gd, Tb, Dy, Ho, Er, and Lu, by the same route as previously described for the Dy compound. Since the Gd and Tb samples still contained large amounts of the 2:17 phase (about 20 wt %) and these could not be decreased by composition adjustment or annealing, further investigations were carried on selected samples with R = Dy, Ho, Er and Lu. The latter ones had only minor contents in α-Fe and Th_2Ni_{17}-type secondary phases.

Magnetic measurements were performed on magnetically aligned samples using a Quantum Design MPM5 magnetometer in the temperature range 5–300 K. Cylindrical-shaped samples consisted of powders with a grain size of less than 20 μm, embedded in epoxy resin and aligned in a magnetic field of about 0.5 T, with the axis of the cylinder parallel and perpendicular, respectively, to the field direction, at room temperature. The easy magnetization direction (EMD) at room temperature was inferred from the analysis of the x-ray diffraction patterns of random and magnetic-field aligned powders. In the following, $M_{\parallel}$ and $M_{\perp}$ denote the magnetizations measured with the direction of the applied field parallel and perpendicular, respectively, to the c axis of the cylinder. Magnetic isotherms were measured on oriented samples in fields up to 5 T. In order to check the occurrence of spin reorientation transitions, the thermal variation of magnetization was measured in a field of 0.05 T and the dynamic susceptibilities versus temperature in an ac field with a 4.5 Oe amplitude and 90 Hz frequency.

The saturation magnetization M_s was derived from the 5 K magnetization isotherms measured on free powders, in fields $H \leqslant 5$ T, by extrapolation of $M(1/H^2)$ to $1/H^2 \rightarrow 0$ and subsequent correction for the free iron content as given by the refinement of the x-ray diffraction data, according to the relation $M_{s,extr.} = f_{1:12}M_s + f_{Fe}M_{s,Fe}$; herein, $M_{s,extr.}$ is the saturation magnetization value obtained by extrapolation of the raw data, $M_{s,Fe}$ is the saturation magnetization of iron (221 emu/g at 4.2 K), and $f_{1:12}$ and f_{Fe} are the fractions of 1:12 and α-Fe phases, respectively. The estimated error in the M_s values is $\pm 0.6\mu_B$/f.u., and is due to the uncertainty in the values of $f_{1:12}$ and f_{Fe} fractions.

III. $R\mathrm{Fe}_{11.3}\mathrm{W}_{0.7}$ COMPOUNDS

A. Structure

The x-ray diffraction patterns of the $R\mathrm{Fe}_{11.3}\mathrm{W}_{0.7}$ compounds, experimental and calculated, are plotted in Fig. 1. First, the data were analyzed using the pattern-matching utility provided by the FULLPROF program, in order to obtain initial values for the coefficients of the background polynomial, the zero shift, the lattice parameters, and the peak shape parameters (pseudo-Voigt function). Then Rietveld refinements were performed, with the W and Fe atoms sharing the $8i$ sites, as systematically observed for T being an nd type transition element. Full occupancies of the $8j$ and $8f$ sites by iron and the $2a$ site by the rare earth were assumed (see the inset in Fig. 1). The scale factor, zero shift, lattice parameters, atomic positions, and the peak shape parameters were progressively introduced as fitting parameters. The occupation number and overall isotropic temperature factors were finally refined. The α-iron content in the samples, as given by the refinement, is 6, 8, 4.5, and 4 wt. %, for R = Dy, Ho, Er, and Lu, respectively. Additionally, characteristic reflections of the 2-17 phase were identified only for R = Ho and Lu, giving amounts of 5 wt. % in both cases. The discrepancies between the fits and the experimental patterns at around 43°, in all samples, cannot be attributed to the 2-17 secondary phase; instead, this may be assigned to a persistent texture of 1-12 phase, though this could not be accounted for with the simple texture functions implemented in the fitting program. Table I displays the structural parameters, the refinement reliability factors, and the interatomic distances less than 3.5 Å. It may be observed that the unit cell decreases in the trend R = Dy to Lu, reflecting the lanthanides contraction, whereas the c/a ratio remains approximately constant, $c/a = 0.56$, which indicates isotropic lattice constants variations, as generally found for Fe-rich 1:12 compounds.[1–12] The refined W content is slightly lower than the nominal stoichiometry (see Table I), which suggests that a small fraction of the W atoms could have been dissolved into the free iron secondary phase.

One may also observe that there are two distinct ranges of Fe-Fe distances: (i) very short ones, less than the critical value $d_0 \approx 2.45$ Å, between the $8i$-$8i$, $8f$-$8f$, and $8j$-$8f$ sites, for which, in a Néel-Slater-type approach the exchange energy between Fe spins is expected to be negative and therefore to favor antiparallel coupling of the spins;[20] and (ii) a range extending from about 2.6 to 2.9 Å, for which the model predicts that the exchange energy between iron spins is positive and leads to their parallel coupling.

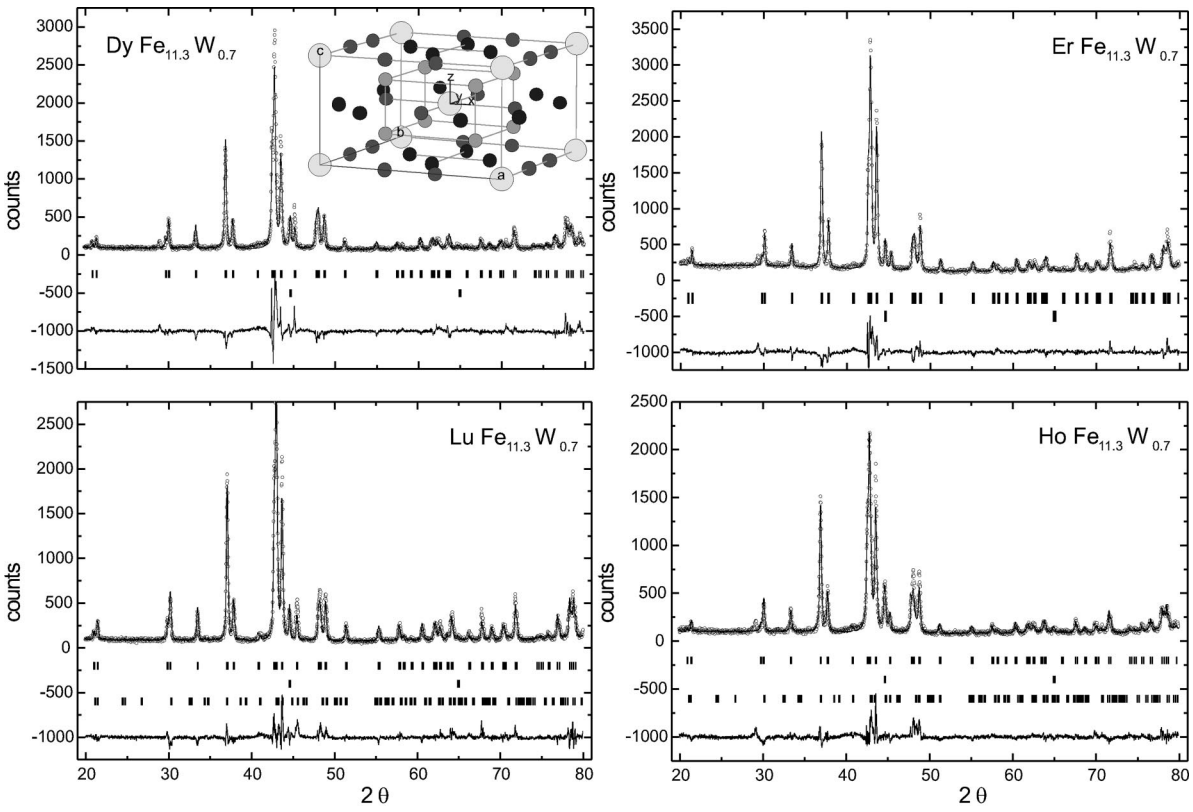

FIG. 1. Experimental, calculated, and difference x-ray diffraction patterns. Inset: the unit cell of the $ThMn_{12}$ structure; large circles: $2a$ sites (R atoms), small circles from light gray to black: $8f$, $8i$, and $8j$ sites (Fe atoms), respectively.

B. Magnetic properties

1. $LuFe_{11.3}W_{0.7}$

The saturation magnetization $M_s=20.1(\pm0.6)\mu_B$/f.u. at 5 K and the Curie temperature $T_C=490(\pm2)$ K (see Table II) may be taken as references for the contributions to magnetization and exchange interactions, respectively, of the iron sublattice (Lu is nonmagnetic) in the $R\mathrm{Fe}_{11.3}\mathrm{W}_{0.7}$ compounds. Within the error, the M_s value is close to that determined in $\mathrm{LuFe}_{11.5}\mathrm{Ta}_{0.5}$, $20.9\mu_B$/f.u.,[3] or $\mathrm{LuFe}_{11.35}\mathrm{Nb}_{0.65}$, $20.6\mu_B$/f.u.[7] The relatively large exchange splitting, which leads to a mean iron moment $M_{Fe}\approx1.8\mu_B$/at., and the low Curie temperature, are characteristic for a quasiweak ferromagnetic, as discussed in Ref. 17. The mean iron moment in $\mathrm{LuFe}_{11.3}\mathrm{W}_{0.7}$ is slightly smaller than that in the $\mathrm{Fe}_{100-z}\mathrm{W}_z$ solid solution, $\sim1.9\mu_B$/f.u. at 5 K, derived by a linear extrapolation of the magnetization data to $z=5.8$.[21]

The thermal variation of magnetization measured between 5 and 300 K and $H=0.05$ T reveals no particular feature which could indicate the occurrence of a spin reorientation transition within the iron sublattice. Actually, the preference of the iron sublattice magnetization for the tetragonal c axis up to T_C was recently firmly determined by magnetic[3] and neutron diffraction[4] studies on $\mathrm{LuFe}_{11.5}\mathrm{Ta}_{0.5}$, and also by magnetic measurements on a variety of $R\mathrm{Fe}_{12-x}T_x$ compounds with R=Y, Lu, and Gd, previously.[1,2]

The magnetization curves measured on oriented samples, at 5 and 300 K, are drawn in Fig. 2(a). The values of the anisotropy constants are listed in Table II, as derived from Sucksmith-Thompson plots without applying the correction for misalignment. The existence of some degree of misalignment and also the presence of the free iron secondary phase in the sample lead to the observed curvature in the $M_\perp(H)$ plots, and to an overestimation of the fourth-order anisotropy constant, K_2.[22]

The anisotropy field H_A, calculated using the relation $\mu_0H_A=(2K_1+4K_2)/M_s$, is 2.4 T at room temperature (RT) and 4.6 T at 5 K, values which are larger than 1.65 and 3.47 T, respectively, obtained using the same method, in $\mathrm{YFe}_{11.3}\mathrm{Nb}_{0.7}$.[12] At RT, a larger anisotropy field, 3 T, was determined in $\mathrm{LuFe}_{11.5}\mathrm{Ta}_{0.5}$, from the intersection of $M_\parallel(H)$ and $M_\perp(H)$ curves.[3] The 5 K value of $K_1=0.69$ MJ/m^3 (see Table II), is larger than 0.564 MJ/m^3 in $\mathrm{LuFe}_{11.35}\mathrm{Nb}_{0.65}$, whereas the RT value, 0.31 MJ/m^3, is smaller than 0.459 MJ/m^3 for the Nb compound, determined from the polar dependences of the $M_\parallel$ and $M_\perp$ components of magnetization.[11] At any rate, the differences are not large when compared to other $R\mathrm{Fe}_{11.5}\mathrm{Ta}_{0.5}$ and $R\mathrm{Fe}_{11.35}\mathrm{Nb}_{0.65}$ compounds.

2. $DyFe_{11.3}W_{0.7}$

The saturation magnetization $M_s=11.6(\pm0.6)\mu_B$/f.u. at 5 K and the Curie temperature $T_C=533(\pm2)$ K (see Table II) were determined for the Dy compound. The comparison of the M_s value to that determined in $\mathrm{LuFe}_{11.3}\mathrm{W}_{0.7}$ evidences a ferrimagnetic-type coupling between the iron and the Dy magnetic sublattices, as expected.

TABLE I. Lattice constants a and c, their ratio, unit-cell volume, $V_{u.c.}$, Fe/W(8i) and Fe(8j) atomic positions, x, Fe(8i) and W(8i) fractional occupancies n, overall temperature factor, reliability factors R_{wp}, χ^2 and R_B, interatomic distances, d, and average FeFe distances d_{FeFe} in $R\mathrm{Fe}_{11.3}\mathrm{W}_{0.7}$ compounds.

	$\mathrm{DyFe}_{11.3}\mathrm{W}_{0.7}$	$\mathrm{HoFe}_{11.3}\mathrm{W}_{0.7}$	$\mathrm{ErFe}_{11.3}\mathrm{W}_{0.7}$	$\mathrm{LuFe}_{11.3}\mathrm{W}_{0.7}$
a (Å)	8.5156(4)	8.5009(3)	8.4898(4)	8.4627(2)
c (Å)	4.7705(3)	4.7657(2)	4.7632(3)	4.7553(2)
c/a	0.560	0.561	0.561	0.562
$V_{u.c.}$ (Å^3)	345.9(0)	344.4(0)	343.3(0)	340.6(0)
Fe/W(8i), x	0.3608(5)	0.3597(4)	0.3587(6)	0.3602(3)
Fe(8j), x	0.2764(7)	0.2791(6)	0.2845(8)	0.2811(5)
n_{Fe}(8i)	0.824(0)	0.832(0)	0.836(0)	0.832(0)
n_W(8i)	0.176(0)	0.168(0)	0.164(0)	0.168(0)
B	0.24(8)	0.52(7)	0.22(9)	0.21(6)
R_{wp}	18.7	13.4	11.9	13.8
χ^2	6.04	3.04	3.67	3.41
R_B	14.7	10.9	11.8	11.3
$d_{8i\text{-}8i}$ (Å)	2.371(6), 2.916(2)	2.385(5), 2.919(2)	2.398(7), 2.924(3)	2.367(4), 2.908(2)
$d_{8i\text{-}8j}$ (Å)	2.635(3), 2.656(3)	2.655(3), 2.659(3)	2.674(4), 2.696(4)	2.657(2), 2.661(2)
$d_{8i\text{-}8f}$ (Å)	2.616(1)	2.609(1)	2.603(2)	2.600(1)
$d_{8j\text{-}8j}$ (Å)	2.693(6)	2.656(5)	2.588(7)	2.620(4)
$d_{8j\text{-}8f}$ (Å)	2.451(1)	2.449(1)	2.451(1)	2.441(0)
$d_{8f\text{-}8f}$ (Å)	2.385(0)	2.383(0)	2.382(0)	2.378(0)
$d_{8i\text{-}2a}$ (Å)	3.072(4)	3.058(4)	3.046(5)	3.048(3)
$d_{8j\text{-}2a}$ (Å)	3.052(4)	3.034(3)	3.003(4)	3.014(3)
$d_{8f\text{-}2a}$ (Å)	3.238(0)	3.233(0)	3.229(0)	3.220(0)
$d_{Fe\text{-}Fe,8i}$ (Å)	2.699	2.702	2.711	2.695
$d_{Fe\text{-}Fe,8j}$ (Å)	2.577	2.574	2.572	2.567
$d_{Fe\text{-}Fe,8f}$ (Å)	2.504	2.500	2.498	2.492

The analysis of the x-ray diffraction peaks measured on random as well as magnetic field aligned powders allowed us to assess that the EMD lies along the c axis in the $\mathrm{DyFe}_{11.3}\mathrm{W}_{0.7}$ at RT, as previously determined for $\mathrm{DyFe}_{12-x}T_x$ with T=Ta,[3,4] Nb,[7] Ti,[2] and Mo.[23] When cooling down, a broad peak in the $\chi'_{\parallel}(T)$ curve appears at about 275 K [Fig. 3(a)], and also is evidenced in the thermal variations of magnetization, more prominently on the $M_{\parallel}(T)$ curve [Fig. 4(a)]. We associate this peak with the occurrence of a spin reorientation transition from an easy c axis to an easy cone, at $T_{SR1}\approx 275$ K, as already established in $\mathrm{DyFe}_{11.5}\mathrm{Ta}_{0.5}$ at $T_{SR1}=265$ K,[3,4] $\mathrm{DyFe}_{11.35}\mathrm{Nb}_{0.65}$ at $T_{SR2}=235$ K,[7] and $\mathrm{DyFe}_{11}\mathrm{Ti}$ at $T_{SR2}\sim 200$–240 K.[24] Below T_{SR1} the magnetizations $M_{\parallel}(T)$ and $M_{\perp}(T)$ decrease smoothly and mimic the temperature dependence of the spontaneous magnetization. However, one may observe a broad peak at ~ 140 K on the $\chi''_{\parallel}(T)$ curve, plotted in Fig. 3(a), and also observe that the $M_{\parallel}(H)$ curve does not reach saturation in a field up to 5 T, at 5 K [Fig. 2(b)]. Whether or not, below T_{SR1}, the system undergoes a spin reorientation transition from a cone to a basal plane—with the lack of a clear indication of T_{SR2} on the thermal variations of magnetizations $M_{\parallel}(T)$ or $M_{\perp}(T)$, except for a change in slope at about 160 K on the $M_{\parallel}(T)$ curve—is worthy of comment.

Recently, neutron diffraction results obtained on $\mathrm{DyFe}_{11.5}\mathrm{Ta}_{0.5}$ (Ref. 4) showed that the magnetization is already confined to the basal plane at 200 K, a temperature which is above that corresponding to the second change in slope, 185 K, on the $M_{\perp}(T)$ curve [see Fig. 3-(top) in Ref. 3]. Therefore, the temperature T_{SR2} for the onset of the cone

TABLE II. Magnetic data of $R\mathrm{Fe}_{11.3}\mathrm{W}_{0.7}$ compounds.

R	T_C (K) ± 2 K	$M_s(\mu_B$/f.u.) ± 0.6 μ_B/f.u.	T_{SR} (K)	K_1 (MJ/m^3) 300 K	K_2 (MJ/m^3) 300 K	H_A 300 K	K_1 (MJ/m^3) 5 K	K_2 (MJ/m^3) 5 K	H_A (T) 5 K
Dy	533	11.6	275	0.27	0.20	1.5	−0.69	0.22	0.6
Ho	521	13.2	-	0.08	0.65	2.8	0.36	0.28	2.4
Er	506	12.3	45	0.28	0.59	3.7	-	-	-
Lu	490	20.1	-	0.31	0.38	2.4	0.69	0.99	4.6

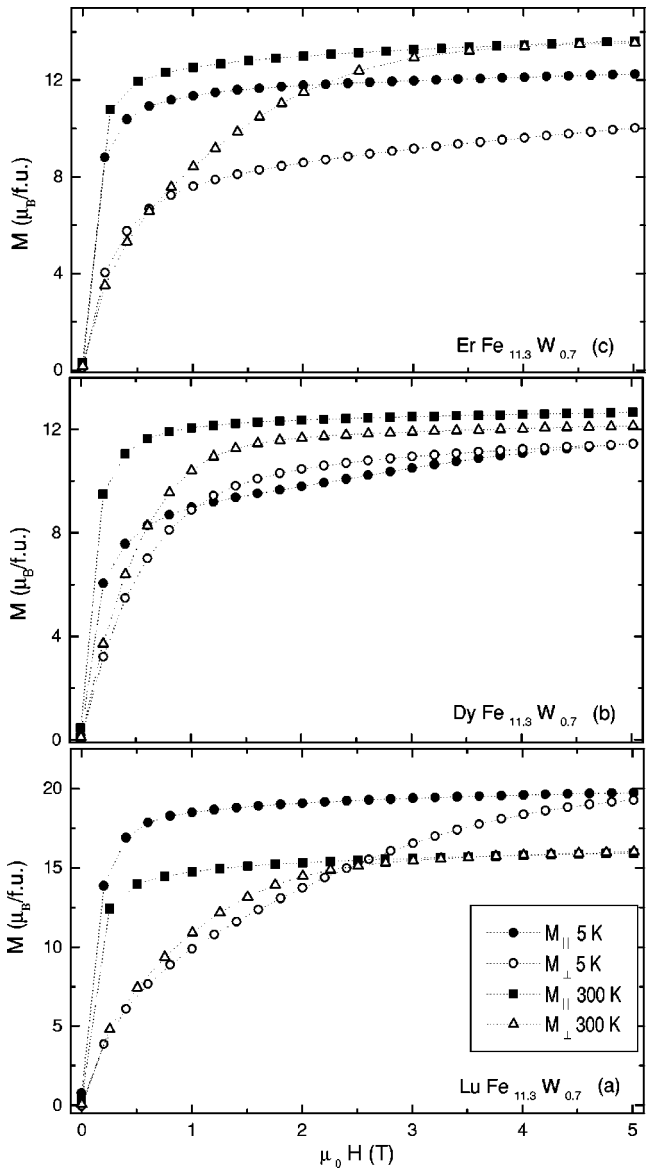

FIG. 2. Magnetic-field dependencies of $M_{\parallel}$ and $M_{\perp}$ at 5 and 300 K for $\mathrm{LuFe}_{11.3}\mathrm{W}_{0.7}$ (a), $\mathrm{DyFe}_{11.3}\mathrm{W}_{0.7}$ (b), and $\mathrm{ErFe}_{11.3}\mathrm{W}_{0.7}$ (c).

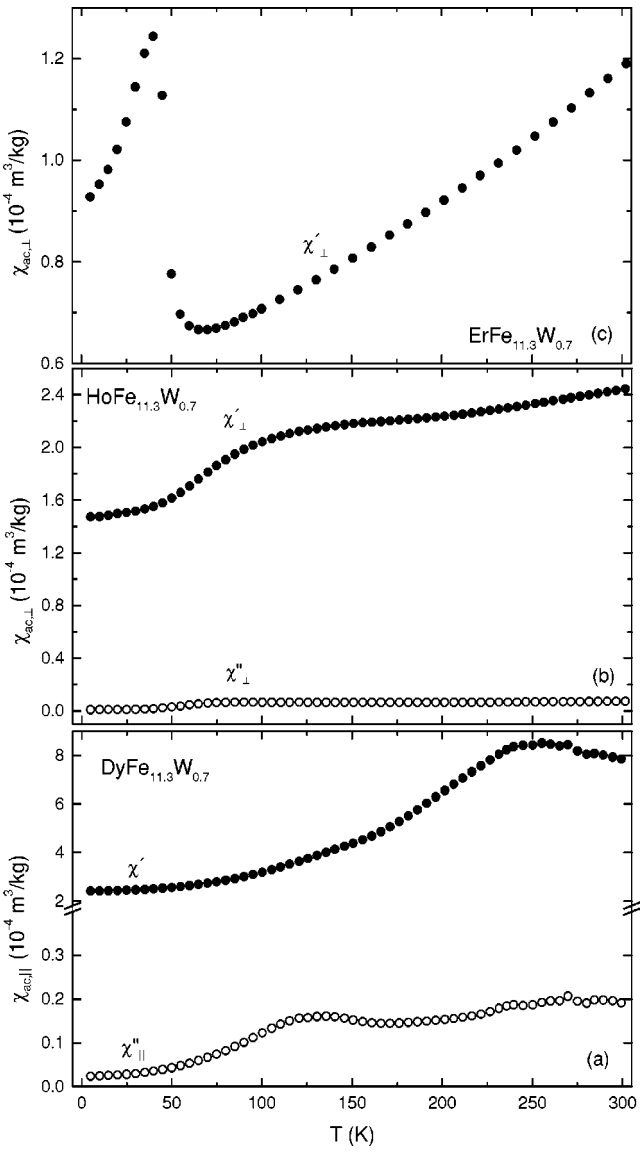

FIG. 3. Temperature dependencies of the ac susceptibility of $\mathrm{DyFe}_{11.3}\mathrm{W}_{0.7}$ (a), $\mathrm{HoFe}_{11.3}\mathrm{W}_{0.7}$ (b), and $\mathrm{ErFe}_{11.3}\mathrm{W}_{0.7}$ (c).

to in-plane spin reorientation transition has been taken as 210 K, which corresponds to the first change in slope of the $M_{\perp}(T)$ curve, below T_{SR1}. Although the cone-to-basal-plane EMD transition is of first-order type, it takes place gradually, between 210 and 185 K, in $\mathrm{DyFe}_{11.5}\mathrm{Ta}_{0.5}$.[4] This type of behavior has been explained by assuming the coexistence of two volume fractions of the conical and basal phases in that thermal range, such that their relative extents and average angle, respectively, evolve continuously with temperature. Previously, such a phenomenology was used to explain the spin reorientation transitions in the $\mathrm{DyFe}_{11}\mathrm{Ti}$ single crystal,[24] and recently, a model based on the structural disorder, characteristic of 1:12 phases, was developed to account for the coexistence of domains with easy-cone- and easy-plane-type anisotropies.[25]

Therefore, the present $\chi_{\parallel}''(T)$ and $M_{\parallel}(T)$ data for the $\mathrm{DyFe}_{11.3}\mathrm{W}_{0.7}$ compound may be interpreted as showing that the system undergoes a progressive, first-order spin reorientation transition from easy cone to easy plane, with the onset of the transition at $T_{SR2}\approx 200$ K. Due to the similarity with $\mathrm{DyFe}_{11.5}\mathrm{Ta}_{0.5}$, we suggest that the transition is complete at the temperature where the peak in $\chi_{\parallel}''(T)$ and the change in slope in $M_{\parallel}(T)$ curves are observed, $T'_{SR2}\sim 140$–160 K. Below T'_{SR2} the basal plane becomes an easy magnetization plane. The magnetization isotherms $M_{\parallel}(H)$, plotted in Fig. 5(a), reveal the occurrence of a first-order magnetization process (FOMP) at a critical field $\mu_0 H_{cr}\leqslant 2.5$ T and up to a critical temperature $T_{cr}\approx 70$ K [see the inset of Fig. 5(a)] in the proposed thermal range of the easy-plane anisotropy. The magnetization direction changes from a basal plane to a cone in an applied field perpendicular to the easy plane. Also, a careful observation of the 100, 200, and 300 K isotherms shows that the shape of the 100 K isotherm is different from the higher-temperature ones, approaching saturation along the c axis, which is of hard magnetization at 100 K at a

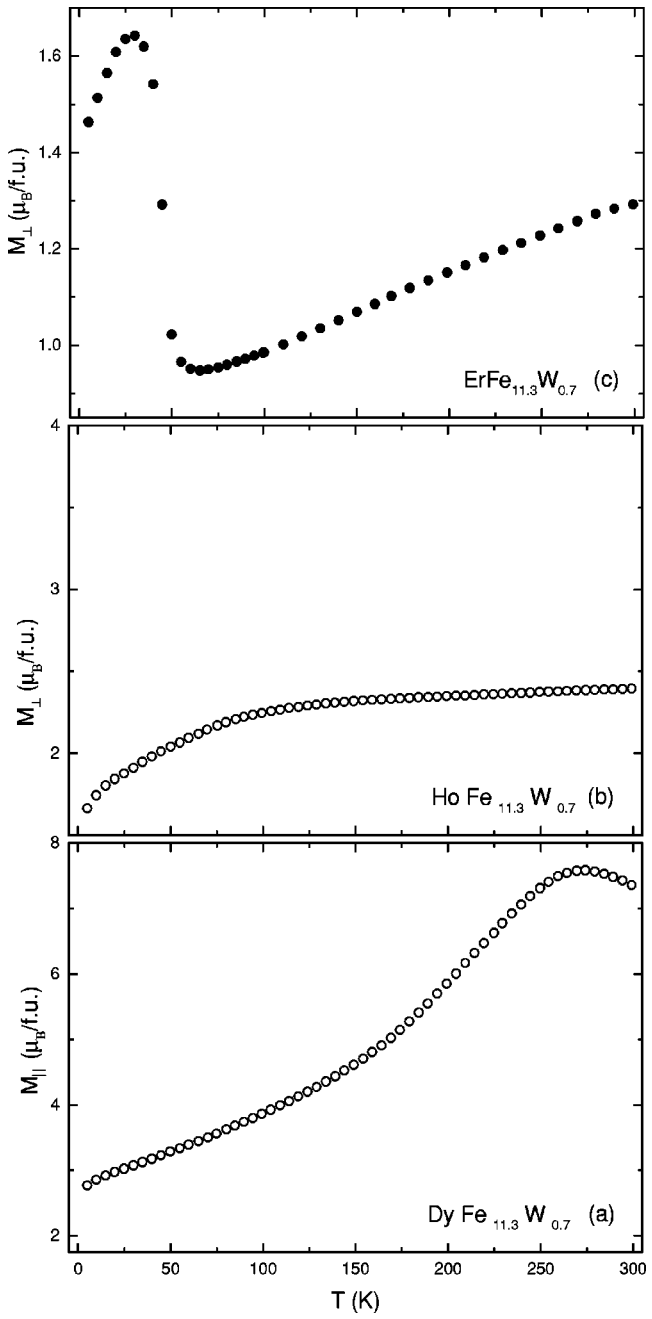

FIG. 4. Temperature dependencies of magnetization of $DyFe_{11.3}W_{0.7}$ (a), $HoFe_{11.3}W_{0.7}$ (b), and $ErFe_{11.3}W_{0.7}$ (c), in an applied field $\mu_0 H = 0.05$ T.

higher field. At room temperature, the anisotropy field $\mu_0 H_A = 1.5$ T (see Table II) is smaller than in the Lu compound, suggesting a persistent, negative contribution to K_1 from the Dy sublattice. At 5 K, an anisotropy field of 0.6 T is obtained using the expression $\mu_0 H_A = -(2K_1 + 4K_2)/M_s$ for the in-plane anisotropy.

3. $HoFe_{11.3}W_{0.7}$

Temperature scans of the ac susceptibility $\chi'_\perp(T)$ [Fig. 3(b)], and of the magnetization, $M_\perp(T)$ [Fig. 4(b)], reveal no anomalous behavior, and therefore it may be derived that

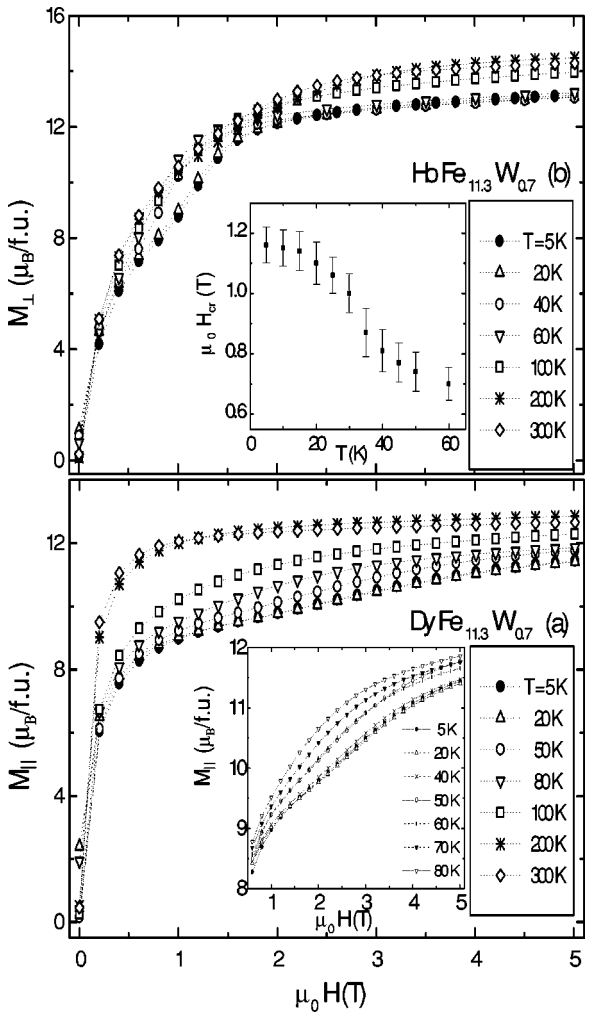

FIG. 5. Selected magnetization isotherms in the temperature range 5–300 K, of $DyFe_{11.3}W_{0.7}$ (a) and $HoFe_{11.3}W_{0.7}$ (b). Inset (a): Enlarged plot of the $M(H)$ curves between 5 and 80 K, to show the FOMP in $DyFe_{11.3}W_{0.7}$. Inset (b): Temperature dependence of the critical field, $H_{cr.}(T)$ in $HoFe_{11.3}W_{0.7}$.

the EMD preserves its *c*-axis orientation, determined at RT from x-ray diffraction patterns on oriented powders, down to 5 K. The saturation magnetization has the value $M_s = 13.2\ (\pm 0.6)\mu_B$/f.u. at 5 K and the Curie temperature $T_C = 521\ (\pm 2)$ K (see Table II). Selected magnetization versus field curves, $M_\perp(H)$, at several temperatures in the range 5–300 K, are presented in Fig. 5(b). A first-order magnetization process is observed to occur below ~ 70 K, with a maximum critical field $\mu_0 H_{cr} \sim 1.2$ T at 5 K. Both the FOMP critical temperature T_{cr} and the maximum critical field are smaller than the values $T_{cr} \approx 125$ K and $\mu_0 H_{cr} = 1.7$ T, respectively, determined in the $HoFe_{11.5}Ta_{0.5}$ compound.[3] The temperature dependence of the critical field is plotted in the inset of Fig. 5(b).

The anisotropy field decreases slightly, from 2.8 to 2.4 T, when cooling down from 300 to 5 K. Nevertheless, the anisotropy data for the Lu compound show that the uniaxial anisotropy of the iron sublattice attains a significant enforcement when decreasing the temperature. Therefore, the small decrease observed in H_A at 5 K relative to RT, in

$\mathrm{HoFe}_{11.3}\mathrm{W}_{0.7}$, is due to the competition between the Fe sublattice contribution, favoring the *c* axis, and the Ho sublattice contribution, which increasingly favors an in-plane anisotropy at low *T*, as expected in $R(\mathrm{Fe},T)_{12}$ for the rare earths with negative second-order Stevens coefficient, α_J.

4. $ErFe_{11.3}W_{0.7}$

In the case of $\mathrm{ErFe}_{11.3}\mathrm{W}_{0.7}$, a saturation magnetization $M_s=12.3(\pm 0.6)\mu_B$/f.u. at 5 K and a Curie temperature $T_C=506(\pm 2)$ K were determined. The Er compound undergoes a spin reorientation transition at $T_{SR}=45$ K when cooling down from 300 K, as evidenced by the sharp peaks which appear on both the ac susceptibility $\chi'_{ac,\perp}(T)$ [Fig. 3(c)], and magnetization $M_\perp(T)$ [Fig. 4(c)], curves. The transition is from a uniaxial phase to a conical phase, and was also observed in $\mathrm{ErFe}_{11.5}\mathrm{Ta}_{0.5}$ at $T_{SR}=40$ K.[4] Such a transition in a system in which the Fe sublattice has a uniaxial anisotropy and Er has $\alpha_J>0$, which also favors the *c*-axis EMD, is due to the increasing influence with decreasing temperature of the higher-order terms in the crystalline electrostatic field expansion, which favor other directions as easy axis.[7] The magnetization curves $M_\parallel(H)$ and $M_\perp(H)$ at 5 and 300 K are plotted in Fig. 2(c). At 300 K the anisotropy field $H_A=3.7$ T (see Table II) is significantly larger than in the Lu compound due to the contribution of the erbium sublattice to the uniaxial anisotropy. At 5 K one may observe that the magnetization along the perpendicular direction does not reach saturation in fields up to 5 T.

IV. *nd*-4*f* EXCHANGE IN THE $R(\mathrm{Fe},T)_{12}$ CLASS OF COMPOUNDS

A. Mean-field exchange parameters

The *R*-Fe and Fe-Fe exchange interactions were estimated assuming a negligibly small *R*-*R* exchange, and assuming that the Fe-Fe exchange across the lanthanide series is that in the Lu compound. In the mean field approximation, in the magnetic order temperature range, the exchange integrals J_{ij}, the exchange coefficients n_{ij} (reflecting the interactions between *R* and Fe spin magnetic moments), and the exchange fields $H_{ex,i}$, $(i,j=R,\mathrm{Fe})$ are given by the equations[26,27]

$$J_{FeFe}=\frac{3k_BT_C^0}{2Z_{FeFe}S_{Fe}^0(S_{Fe}^0+1)}, \tag{1a}$$

$$J_{RFe}=3k_B\left[\frac{T_C(T_C-T_C^0)}{4Z_{RFe}Z_{FeR}S_{Fe}(S_{Fe}+1)G_J}\right]^{1/2}, \tag{1b}$$

$$n_{FeFe}=\frac{Z_{FeFe}J_{FeFe}}{2N_{Fe}\mu_B^2}, \tag{2a}$$

$$n_{RFe}=\frac{Z_{RFe}J_{RFe}}{2N_{Fe}\mu_B^2}, \tag{2b}$$

TABLE III. Exchange interaction parameters in $R\mathrm{Fe}_{11.3}\mathrm{W}_{0.7}$, in the magnetic order temperature range.

R	J_{FeFe} (10^{-22} J)	J_{RFe} (10^{-22} J)	n_{FeFe} (μ_0)	$-n_{RFe}$ (μ_0)	$H_{ex,Fe}$ (T)	$H_{ex,R}$ (T)
Lu	5.97 (43.3 K)	-	420	-	579	-
Dy	..	1.59 (11.5 K)	..	216	652	148
Ho	..	1.67 (12.1 K)	..	227	640	124
Er	..	1.57 (11.3 K)	..	212	622	97

$$H_{ex,Fe}=\frac{Z_{FeFe}S_{Fe}J_{FeFe}+Z_{FeR}(g_J-1)JJ_{RFe}}{\mu_B}, \tag{3a}$$

$$H_{ex,R}=\frac{2Z_{RFe}(g_J-1)S_{Fe}J_{RFe}}{g_J\mu_B}, \tag{3b}$$

where the superscript (0) refers to the respective quantity in the Lu (or Y) compound, S_{Fe} is the iron spin, k_B is the Boltzmann constant, Z_{ij} represent the average numbers of *j* atoms nearest neighbors to an *i* atom, N_{Fe} and N_R stand for the numbers of Fe and *R* atoms, respectively, per unit volume and μ_B is the Bohr magneton. Also, *J*, g_J, and G_J are the total angular momentum, the Landé factor, and the de Gennes factor, respectively, of the rare-earth atom. The calculation of Z_{ij} in $R\mathrm{Fe}_{11.3}\mathrm{W}_{0.7}$ using a binomial probability of local environments, with the W atoms distributed over the $8i$ sites, yields the values $Z_{RFe}=19.3$, $Z_{FeR}=1.7$, and $Z_{FeFe}=10.1$. The exchange parameters calculated using Eqs. (1)–(3), and $S_{Fe}^0=0.89$ derived from the 5 K mean iron moment $M_{Fe,Lu}=1.78\mu_B$/at., are listed in Table III. Their values are in the ranges determined by the same method in other iron-rich rare-earth intermetallics.[5,10,11,28]

In order to allow for further discussion on exchange by comparison to other $R\mathrm{Fe}_{12-x}T_x$ compounds, we also have estimated n_{FeFe} and n_{RFe} in the paramagnetic domain, using the equations[29]

$$n_{FeFe}=\frac{T_C^0}{C_{Fe}}, \tag{4a}$$

$$n_{RFe}=\frac{\sqrt{T_C(T_C-T_C^0)}}{\gamma\sqrt{C_RC_{Fe}}}, \tag{4b}$$

where the Curie constants are given by $C_{Fe}=N_{Fe}p_{eff,Fe}^2\mu_B^2/3k_B$ and $C_R=N_Rp_{eff,R}^2\mu_B^2/3k_B$ and $\gamma=2(g_J-1)/g_J$. We have taken for the effective iron moment $p_{eff,Fe}$, the value $3.7\mu_B$, and the free-ion values for the effective moment of the rare earths, $p_{eff,R}$. The values of n_{FeFe} and n_{RFe}, obtained using Eqs. (4), are listed in Table IV, together with the data for $T=$Ta,[3,5] Re,[30] Nb,[7–11] and Ti (Ref. 16) compounds.

Since there were no data reported for the $\mathrm{LuFe}_{10.8}\mathrm{Re}_{1.2}$ compound, we have estimated its Curie temperature, 412 ± 6 K, by a de Gennes scaling of T_C according to $T_C=T_C^0+6.6G_J$, where the slope is the weighted average of the slopes determined for the W, Ta,[3] and Nb (Ref. 7) series. In the last column of Table IV we list the n_{RFe} values derived

TABLE IV. Values for T_C (in K) and n_{RFe} (in μ_0 units) for some series of $R\mathrm{Fe}_{12-x}T_x$ compounds with heavy rare-earth elements, $x \leqslant 1.2$.

R	$R\mathrm{Fe}_{11.3}\mathrm{W}_{0.7}$ [a]		$R\mathrm{Fe}_{11.5}\mathrm{Ta}_{0.5}$ [b]		$R\mathrm{Fe}_{11.5}\mathrm{Ta}_{0.5}$ [c]		$R\mathrm{Fe}_{10.8}\mathrm{Re}_{1.2}$ [d]		$R\mathrm{Fe}_{11.35}\mathrm{Nb}_{0.65}$ [e]		$R\mathrm{Fe}_{11.35}\mathrm{Nb}_{0.65}$ [f]		$R\mathrm{Fe}_{11}\mathrm{Ti}$ [g]		R-Fe [h]
	T_C	$-n_{RFe}$	T_C	$-n_{RFe}$	T_C	$-n_{RFe}$	T_C	$-n_{RFe}$	T_C	$-n_{RFe}$	T_C	$-n_{RFe}$	T_C	$-n_{RFe}$	$-n_{RFe}$
Gd	-	-	-	-	-	-	-	-	597	172	600	174	607	178	169
Tb	-	-	576	171	568	153	475	145	556	159	553	154	554	151	154
Dy	533	150	550	176	547	150	-	-	536	160	534	154	534	151	145
Ho	521	158	541	183	526	130	448	162	520	160	523	167	520	157	132
Er	506	150	532	217	520	146	-	-	507	162	509	169	505	149	125
Tm	-	-	-	-	507	80	-	-	-	-	-	-	496	146	117
Lu	490	-	499	-	505	-	412	-	489	-	488	-	488	-	-
n_{FeFe}^{Lu}	207		211		210		206 [i]		210		225 [i]		215		

[a]This work
[b]Reference 3.
[c]Reference 5.
[d]Reference 30.
[e]References 7–9.
[f]References 10 and 11.
[g]Reference 16.
[h]Reference 31.
[i]For the Y compound.

from the intra-atomic exchange integrals obtained by self-consistent relativistic atomic calculations.[31] In order to investigate the trend in the dependence of the intersublattice exchange in $R\mathrm{Fe}_{12-x}T_x$ on the type and rate of transition metal substitution for Fe, we have calculated using Eqs. (4) the exchange coefficients for $R\mathrm{Fe}_{10.5}\mathrm{Mo}_{1.5}$,[32] and $R\mathrm{Fe}_{10}T_2$,[2] series, T=V and Cr, and the relevant data are listed in Table V.

B. Three sublattice model of exchange

The T_C values of the $R\mathrm{Fe}_{11.3}\mathrm{W}_{0.7}$ compounds, listed in Table II, are systematically smaller than in the corresponding members of the $R\mathrm{Fe}_{11.5}\mathrm{Ta}_{0.5}$ series,[3,5] but, within the experimental errors, the same as those determined in $R\mathrm{Fe}_{11.35}\mathrm{Nb}_{0.65}$ (Refs. 7–11) and $R\mathrm{Fe}_{11}\mathrm{Ti}$.[16] This is outlined in Fig. 6, which displays the Curie temperature versus the unit-cell volume $V_{u.c.}$ One may also observe that, for a given T element, there is a trend in the T_C to increase both with volume and the de Gennes factor. On the other hand, for a given R element, and except for the Ta compounds, T_C appears to be independent of the volume and T element concentration (x=1.0 for Ti and $x \approx 0.7$ for W and Nb). Actually, an increase in T_C with increasing volume and decreasing x should be expected,[1,2] which is fulfilled by the Ta compounds with respect to the Ti compounds. In view that all these compounds present the same crystallographic structure, with the T atoms located only at the $8i$ sites, the fact that the T_C values are fairly the same for the W, Nb, and Ti series, irrespective of volume and x, suggests an interplay between size effects, produced by the

TABLE V. Values for T_C (in K) and n_{RFe} (in μ_0 units) for some series of $R\mathrm{Fe}_{12-x}T_x$ compounds, $x \geqslant 1.5$.

R	$R\mathrm{Fe}_{10.5}\mathrm{Mo}_{1.5}$ [a]		$R\mathrm{Fe}_{10}\mathrm{Mo}_2$ [b]		$R\mathrm{Fe}_{10}\mathrm{V}_2$ [b]		$R\mathrm{Fe}_{10}\mathrm{Cr}_2$ [b]	
	T_C	$-n_{RFe}$	T_C	$-n_{RFe}$	T_C	$-n_{RFe}$	T_C	$-n_{RFe}$
Gd	460	159	430	198	616	205	580	197
Tb	430	158	390	199	570	195	525	169
Dy	420	179	365	211	540	186	495	154
Ho	410	205	345	230	525	197	485	167
Er	380	185	310	222	505	185	475	189
Tm	375	248	290	245	496	207	465	213
Lu	350	-	260	-	483	-	450	-
n_{FeFe}^{Lu}	160		126		230		211	

[a]Reference 32.
[b]Reference 2.

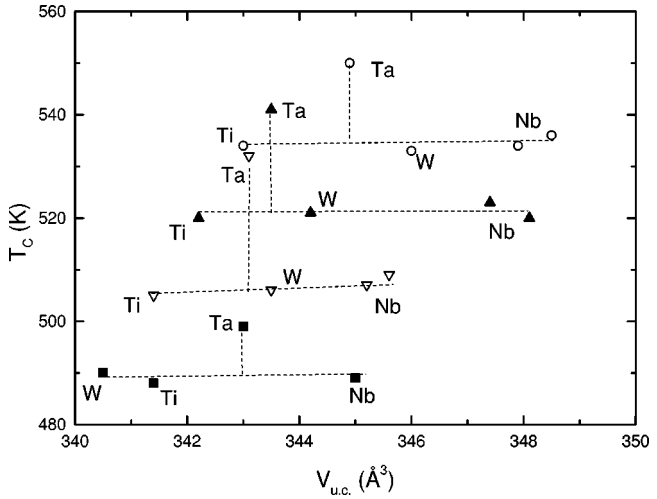

FIG. 6. Curie temperature versus unit cell volume for the $R\mathrm{Fe}_{12-x}T_x$ series in Table IV (■) R=Lu, (○) R=Dy, (▲) R=Ho, and (▽) R=Er (the dashed lines are a guide to the eye).

accommodation of the T atom in the crystal lattice, and the associated electronic effects by the modification of the electronic charge distributions.

In $R\mathrm{Fe}_{12-x}T_x$ compounds, for a given R partner and variable T element, the outer electron configuration of the T atom may induce specific local perturbations of the conduction or valence electron density relative to the ideal $R\mathrm{Fe}_{12}$. Actually, $T(nd)$-Fe$(3d)$ and T(nd)-$R(5d)$ state hybridizations appear supplementary to the Fe$(3d)$-$R(5d)$-hybridzations, and one may presume that an effect upon the exchange couplings should be present relative to the binary compound.

In order to account for the effect of the conduction band electrons on exchange in a mean field analysis, we use the model proposed by Li and Coey[31] (at $T>T_C$), which universally describes the rare-earth $3d$ transition-metal exchange occurring in binary $3d$-$4f$ intermetallics, and which is independent of the specific crystallographic structure due to its atomic nature. In this model, the $4f$ spin couples to the $3d$ spin through the intermediary of the $5d$, $6s$, and $6p$ conduction electrons at the rare-earth site, and the corresponding exchange parameter is

$$n_{RFe}=\chi_c'\frac{J_{4f\text{-}c}}{4N_R\mu_B^2}\left(\frac{J_{3d\text{-}3d}}{4N_{Fe}\mu_B^2}\frac{J_{c\text{-}c}}{4N_R'\mu_B^2}\right)^{1/2}. \tag{5}$$

$J_{4f\text{-}c}$ accounts for the local intra-atomic exchange between the $4f$ electrons and the $5d$, $6s$, and $6p$ electrons, and has been defined as an effective exchange integral,

$$J_{4f\text{-}c}=(n_{5d}J_{4f\text{-}5d}+n_{6s}J_{4f\text{-}6s}+n_{6p}J_{4f\text{-}6p})/n, \tag{6}$$

where n_{nl} is the occupation number of the nl electron band, and $n=n_{5d}+n_{6s}+n_{6p}$. For the trivalent R ions in RFe compounds, $n=3$. The intra-atomic exchange integrals $J_{4f\text{-}nl}$ have been evaluated from self-consistent relativistic calculations.[31] Because the terms $n_{6s}J_{4f\text{-}6s}$ and $n_{6p}J_{4f\text{-}6p}$ appearing in expression (6) bring contributions of about 10% and 3%, respectively, relative to $n_{5d}J_{5d\text{-}5d}$ (see Table 2 in Ref. 31) and also for comparison purposes within an isostructural series, in the following we approximate $J_{4f\text{-}c}\approx(n_{5d}/n)J_{4f\text{-}5d}$. In a similar way, the exchange integral $J_{c\text{-}c}$ between the $5d(6s,6p)$ conduction band electrons within the R sphere (to which the $5d$-$5d$ interaction makes the dominant contribution) has been defined as

$$J_{c-c}=(n_{5d}J_{5d\text{-}5d}+n_{6s}J_{6s\text{-}6s}+n_{6p}J_{6p\text{-}6p})/n\approx\left(\frac{n_{5d}}{n}\right)J_{5d\text{-}5d}, \tag{7}$$

χ_c' is the exchange enhanced susceptibility of the $5d$,$6s$, and $6p$ conduction band electrons. It may be calculated from the Pauli susceptibility χ_c and the intra-band exchange coefficient $n_{c\text{-}c}$,

$$\chi_c'=\frac{\chi_c}{1-\chi_c n_{c\text{-}}}, \tag{8}$$

$$n_{c\text{-}c}=\frac{J_{c\text{-}c}}{4N_R'\mu_B^2}, \tag{9}$$

where χ_c is directly derived from the density of states $N(\varepsilon_F)$ at the Fermi energy ε_F in the free-electron-gas approximation:

$$\chi_c=2\mu_B^2N(\varepsilon_F),\quad N(\varepsilon_F)=\frac{3\rho}{2\varepsilon_F},\quad \varepsilon_F=\left(\frac{\hbar^2}{2m}\right)(3\pi^2\rho)^{2/3}. \tag{10}$$

For the binary RFe compounds, e.g., the ideal $R\mathrm{Fe}_{12}$, the electron-gas density is $\rho=nN_R'=3N_R'$. $n_{c\text{-}c}$ is obtained from $J_{c\text{-}c}$, which is related to the $5d$-$5d$ exchange constant $J_{5d\text{-}5d}$, and the number of electrons in the $5d$ band, as explained above. Thus, essentially, the dependence of the exchange coefficient n_{RFe} on n_{5d} is given by

$$n_{RFe}=\frac{A}{1-Bn_{5d}}n_{5d}^{3/2}, \tag{11}$$

where

$$A=\frac{N(\varepsilon_F)\sqrt{J_{3d\text{-}3d}J_{5d\text{-}5d}}J_{4f\text{-}5d}}{8\mu_B^2N_{Fe}^{1/2}(nN_R)^{3/2}}, \tag{12}$$

$$B=\frac{N(\varepsilon_F)J_{5d\text{-}5d}}{2nN_R}. \tag{13}$$

Equation (11) predicts that n_{RFe} should increase monotonically with n_{5d}, in the range of physically meaningful values. However, both $J_{4f\text{-}5d}$ and $J_{5d\text{-}5d}$ may also vary with n_{5d}, as shown in the framework of the local-spin-density theory:[33] $J_{4f\text{-}5d}$ slightly increases, and $J_{5d\text{-}5d}$ decreases with increasing energy from the bottom of the $5d$ bands; consequently, a competition between these contributions may arise.

1. Trends in the exchange parameters

An inspection of the n_{RFe} data displayed in Tables IV and V reveals that, within the scatter of the experimental values, there is a trend in the R-Fe intersublattice exchange to be rather constant, for R=Gd to Tm, whereas the calculated n_{RFe} decrease monotonically. Previously, a decrease in the R-Fe and R-R exchange, for R from Pr to Tm, in several classes of rare-earth–iron intermetallics, was explained as follows in the two-sublattice model.[29,34] As a result of the much more rapid contraction in the $4f$ charge density than the $5d$ charge density, the distance $d=r_{5d}-r_{4f}$ was shown to increase for R=Pr to Tm, which accounts for the decrease in the local exchange at the rare-earth site and consequently, the decrease in the R-T and R-R exchange. In the analysis of exchange in $R\mathrm{Fe}_{12-x}T_x$ compounds, one should take into account that the variable density in conduction electrons due to both the different types of stabilizing elements, each with complex outer electron configurations and in different concentrations, is a key parameter. In the following, our approach is that, for an isostructural intermetallic series, the experimental lattice constants and atomic positions reflect the equilibrium conditions under the total electronic and ionic potential. Thus their variations, due to small changes in the number of conduction electrons, should reflect the electronic charge redistribution in the system. Therefore, we

have investigated the trends in the dependencies of r_{5d}, $(r_{5d}-r_{4f})$, and n_{RFe} on the number of conduction electrons per unit cell, in several $R\mathrm{Fe}_{12-x}T_x$ series for which detailed structural results are available: present results for $R\mathrm{Fe}_{11.3}\mathrm{W}_{0.7}$; results for $R\mathrm{Fe}_{11.5}\mathrm{Ta}_{0.54}$ in Ref. 4; those for $R\mathrm{Fe}_{11}\mathrm{Ti}$ in Ref. 2, and references cited therein; for $R\mathrm{Fe}_{11.35}\mathrm{Nb}_{0.65}$, and the lattice constants in Ref. 10; atomic positions for the Ho compound in Ref. 11, and those for $R\mathrm{Fe}_{10.5}\mathrm{Mo}_{1.5}$ in Ref. 32. We have approximated r_{5d} of the rare-earth atom by the radius of the Wigner-Seitz cell at the $2a$ site, $r_{W\text{-}S,R}$. The Wigner-Seitz cell volumes were calculated using BLOKJE software.[35] Metallic radii for a coordination number of 12 of the atoms at the $2a$, $8j$, and $8f$ sites were used, and the weighted average value for the $8i$, because of the Fe and T atom distribution, in that case. We have taken the values $\sqrt{\langle r_{4f}^2\rangle}$ for r_{4f}, with the Dirac-Fock integrals $\langle r_{4f}^2\rangle$ for the trivalent rare-earth ions from Table 5 in Ref. 36.

In Fig. 7(a) we represent the dependence of the Wigner-Seitz radius, $r_{W\text{-}S,R}$, at the rare earth site, as a function of the conduction electron number per unit cell. One may observe a systematic increase in $r_{W\text{-}S,R}$ with the increase in the conduction electron density, which may be explained by a transfer of nd electrons ($n=3$, 4, and 5) from the transition metal Fe/T(nd) to $5d$ states at the R site. According to Brooks' proposed interpretation of Campbell's formulation of the RT exchange [intra-atomic $4f$-$5d$ exchange at the R site and $R(5d)$-$T(nd)$ state hybridization[33]], as a result of the hybridization the electron transfer to the $5d$ states at the R site is promoted. The electron transfer is favored as the difference in energy between the $R(5d)$ states and $T(nd)$ states is smaller, as expected (one should recall that we refer to ''electron transfer'' in the metallic matrix in the sense of the variation in the spatial extent of the electron wave function). We suggest that, by changing the T atom type from a $3d$ element to a $4d$ element to a $5d$ element, the Fe($3d$)/$T(nd)$-$R(5d)$ state hybridization is favored and leads to an increase in n_{5d} and consequently, in R-Fe exchange, as indicated by Eq. (11) and also in Ref. 33.

Further, we plot the dependence of the distance $(r_{W\text{-}S,R}$-$r_{4f})$ versus the number of conduction electrons per unit cell in Fig. 7(b). There is a trend in $(r_{W\text{-}S,R}$-$r_{4f})$ to increase with an increasing number of conduction electrons, which has the effect of decreasing the intra-atomic exchange integral, $J_{4f\text{-}5d}$, and therefore to decrease the R-Fe exchange.[29] An increase in n_{5d} also decreases $J_{5d\text{-}5d}$.[33] Consequently, from the competition between these counteracting effects the slight decrease observed in n_{RFe} may result when increasing the electron density in the conduction band, for T from V to Re, in $R\mathrm{Fe}_{12-x}T_x$, see Fig. 7(c).

The dependence of the Wigner-Seitz cell volume at the inequivalent Fe sites versus the number of conduction-band electrons, plotted in Fig. 8, shows different trends: $V_{W\text{-}S}$ decreases at the $8i$ site, is approximately constant for the $8j$ site and increases at the $8f$ site. Since the T atoms are distributed over the $8i$ sites, one may assume that this site is the most susceptible to the variation in the Fe($3d$)/$T(nd)$-$R(5d)$ state hybridization, and subsequent electron

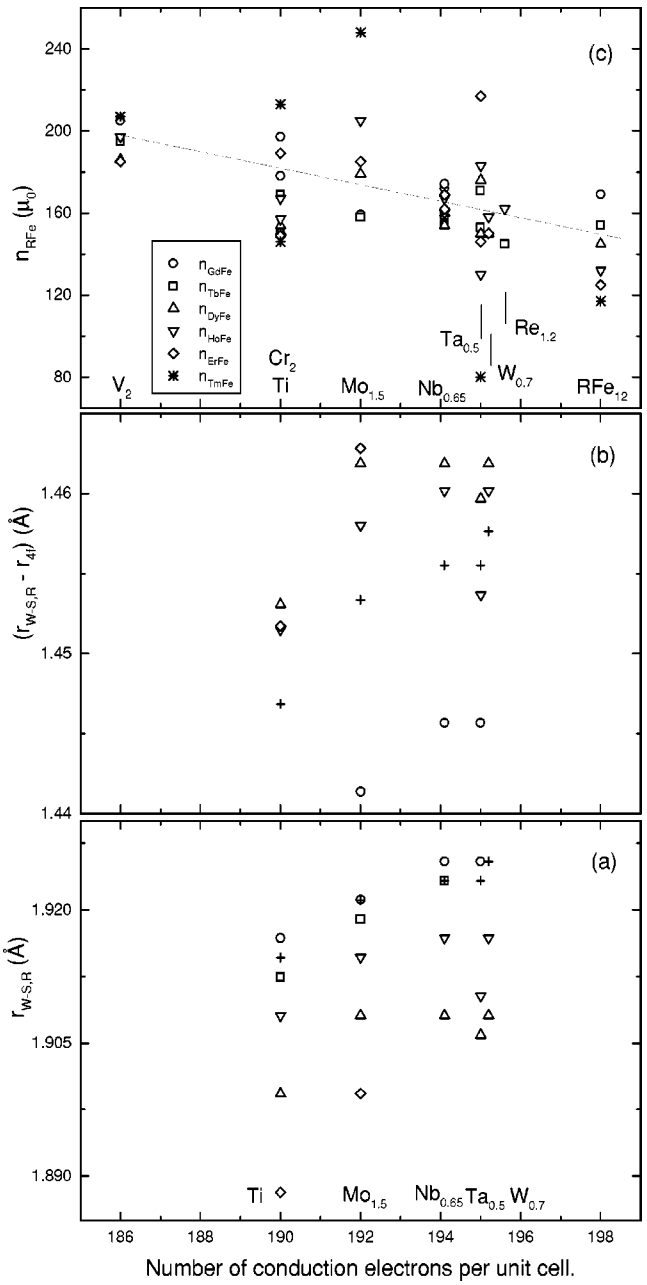

FIG. 7. The dependencies of $r_{W\text{-}S,R}$ (a), $(r_{W\text{-}S,R}-r_{4f})$ (b), and n_{RFe} (c) vs the number of conduction electrons per unit cell (the dashed line is a guide to the eye). For (a) and (b) (□): $R=$Gd; (○): $R=$Tb; (+): $R=$Dy; (△): $R=$Ho; (▽): $R=$Er; and (◇) $R=$Tm.

transfer, although it has only one R-atom nearest neighbor. Therefore, a decrease may be expected in $V_{W\text{-}S,8i}$, as revealed by the data plotted in Fig. 8(a). The $8j$ site, occupied only by Fe and having two R nearest neighbors, is likely to be the least affected by the T atom as regards the $\mathrm{Fe}_{8j}(3d)$-$R(5d)$ state hybridization and the charge transfer involved. The $8f$ site shows trend to increase its volume, which could be either a structural effect, or a size-reflected effect due to a particular scheme of hybridizations, related to the fact that this site is the tightest one in the ThMn_{12} structure.

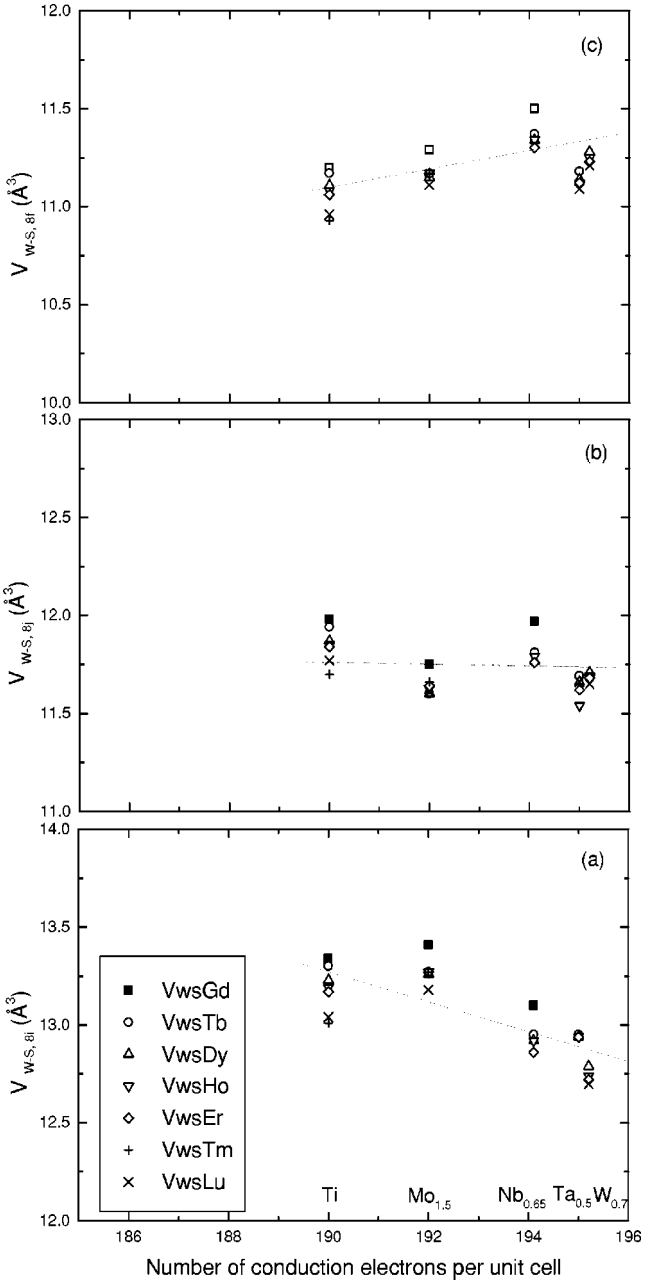

FIG. 8. The dependencies of $V_{W\text{-}S}$ at $8i$ (a), $8j$ (b), and $8f$ (c) vs the number of conduction electrons per unit cell.

We comment that, although the relative variations in $r_{W\text{-}S,R}$ and consequently in $(r_{W\text{-}S,R}-r_{4f})$ with the number of conduction electrons, are small ($\sim$2.5%), they are systematic, and have been derived from experimental data reported by independent groups.

2. nd occupancies

From Eq. (11), using the experimental n_{RFe} values and solving for n_{5d}, one can provide an estimate of the increase in n_{5d} when T is a $5d$ element, e.g., Ta or W, relative to the case when it is a $3d$ element, e.g., Ti, in the $R\mathrm{Fe}_{12-x}T_x$ compounds. Reasonable assumptions about the $3d$-$5d$ and $3d$-$3d$ state hybridizations and electron transfer can be made

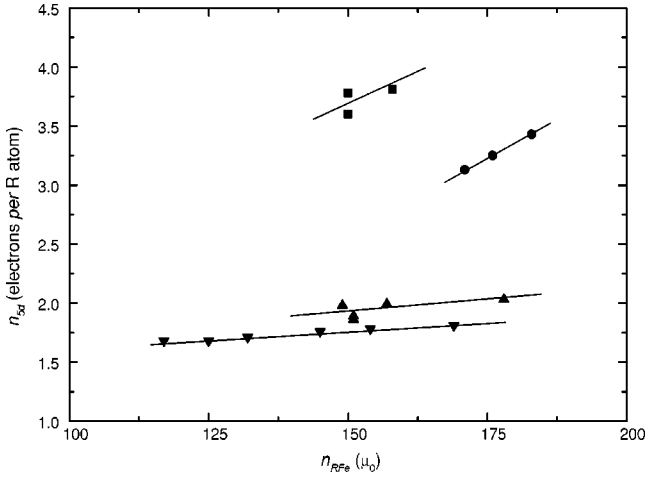

FIG. 9. The $5d$ state population, n_{5d}, vs n_{RFe} in $R\mathrm{Fe}_{11}\mathrm{Ti}$ (▲), $R\mathrm{Fe}_{11.5}\mathrm{Ta}_{0.5}$ (●) and $R\mathrm{Fe}_{11.3}\mathrm{W}_{0.7}$ (■), as calculated using Eq. (11). The values for the binary RFe (▼) were also calculated under the same assumptions.

in these cases, whereas it is hazardous to make any such assumption in the case that T is a $4d$ element (e.g., Nb or Mo) because the $4d$ states have intermediate energies relative to the $3d$ and $5d$ states. We have assumed that Ti $3d$ states behave essentially like Fe $3d$ states (therefore, $n=3$ at the R site, and that Ta or W $5d$ states hybridize mainly with the R $5d$ states (in view of the similar outer electronic configurations of the late rare earths and early $5d$ elements), which yields $n=5.5$ and 7.2 electrons, respectively. We have used the $J_{4f\text{-}5d}$ values listed in Table 2 of Ref. 31, $J_{3d\text{-}3d}=10263$ K and $J_{5d\text{-}5d}=7421$ K.[37] Also, the N_R and N_{Fe} in Eq. (5) were derived from the Wigner-Seitz cell volumes in the present work, $N_R=(V_{W\text{-}S,R})^{-1}$ and $N_{Fe}=(1/3)(V_{W\text{-}S,8i}+V_{W\text{-}S,8j}+V_{W\text{-}S,8f})]^{-1}$, and the value $N'_R=(V_{W\text{-}S,R}+xV_{W\text{-}S,8i})^{-1}$ to account for an enlarged volume for the $J_{c\text{-}c}$ interaction (except for Ti, where obviously $N'_R=N_R$). For comparison, we also obtained the n_{5d} population in binary R-Fe, as explained above, using the calculated n_{RFe} values;[31] in this case, the n_{5d} values turn out to be less than 10% higher than those of Table 2 of Ref. 31. The results of the estimation of n_{5d} at the R site are given in Fig. 9. It is shown that the number of 5d electrons at the R site increases when T=Ta and W relative to Ti compounds. Nevertheless, the fraction n_{5d}/n of $5d$ electrons involved in exchange interaction decreases from about 0.62 for T=Ti, to 0.59 for Ta, and 0.52 for W. When increasing the conduction electron density by changing the T element from Ti to W, higher-energy d states become available at the R site by Fe($3d$)/T(nd)-R($5d$) state hybridizations, which are gradually occupied. Thus the local intra-atomic exchange $J_{4f\text{-}5d}$ and $J_{5d\text{-}5d}$ integrals may vary, at the expense of the correlation energy between the conduction electrons at the R site. We suggest that both the significant increase in n_{5d} from Ti to Ta (see Fig. 9) and the theoretically estimated slight increase in $J_{4f\text{-}5d}$ may lead to the observed increase in n_{RFe}, overweighting the decrease in n_{RFe} produced by the decrease in $J_{5d\text{-}5d}$. However, a further small increase in n_{5d} from Ta to W may not balance the relative larger decrease in $J_{5d\text{-}5d}$,

and this could account for the observed decrease of n_{RFe} from Ta to W. To our knowledge, there are no absorption spectroscopy results on the n_{5d} occupancy in the $R(\mathrm{Fe,T})_{12}$ compounds to compare with the predictions of our analysis.

V. CONCLUSIONS

The structural parameters, Curie temperatures, saturation magnetizations, spin reorientation transitions and strengths of exchange interactions in $R\mathrm{Fe}_{11.3}\mathrm{W}_{0.7}$ compounds, where R=Dy, Ho, Er, and Lu, have been investigated. The iron sublattice behaves as a quasiweak ferromagnetic, shows *c*-axis anisotropy, and couples antiferromagnetically to the heavy rare-earth magnetic sublattice. Dy, Ho, and Er compounds exhibit uniaxial magnetic anisotropies at room temperature, irrespective of the sign of the second-order Stevens coefficient. In the Dy compound an easy-axis–easy-cone spin reorientation is observable at $T_{SR1}=275$ K. As the temperature decreases, a second transition, an easy-cone–easy-plane transition, takes place in a broad temperature range of 200–160 K. Its gradual character is ascribed to the coexistence of two volume fractions of the conical and basal phases, whose relative extents, and average angle of EMD to the *c*-axis, respectively, change continuously with temperature in the transition thermal range. At temperatures below $T_{cr}\approx 70$ K, a first-order magnetization process is observed, with a critical field $H_{cr}\approx 2.5$ T at 5 K. The magnetization direction turns out of the basal plane to a cone when a magnetic field is applied along the *c* axis in this thermal range. In the Ho compound a first-order magnetization process is observed below ~ 70 K, with a critical field $H_{cr}\sim 1.2$ T at 5 K. The Ho sublattice anisotropy is weaker than that of the Dy sublattice, as can be inferred from a comparison of the anisotropy constants and fields relative to the Lu compound (see Table II). A spin reorientation is markedly evidenced at $T_{SR}=45$ K in the $\mathrm{ErFe}_{11.3}\mathrm{W}_{0.7}$ compound. Previously, similar temperature- and field-driven spin reorientation transitions were also reported for corresponding T=Ta, Nb, Mo, and Ti compounds.

An aim of the present work has been to analyze the intersublattice exchange interactions in the $R\mathrm{Fe}_{12-x}\mathrm{T}_x$ class of compounds, with T being an nd-type transition metal ($n=3$, 4, and 5). The conduction band is treated as the third sublattice,[31] and its filling with electrons is considered a varying factor which influences the R-Fe exchange strength. Based on the observed systematic increase of the Wigner-Seitz volume at the R site when increasing the conduction electron density, we assume a concomitant increase in the n_{5d} occupation number. According to Eq. (11), derived in the electron-gas model, the increase in n_{5d} favors the strengthening of the R-Fe exchange. However, this trend is opposed by a decrease in the intra-atomic exchange due to the increase in the $(r_{W\text{-}S,R}-r_{4f})$ distance. From the competition between these effects, a decrease in the exchange coefficient n_{RFe} is apparent; see Fig. 7(c).

In the cases T=Ti, Ta, and W we have derived the n_{5d} electron population at the R site using Eq. (11) and the experimental n_{RFe} values. The increase in n_{5d} from the Ti series to the Ta one correlates with the increase in n_{RFe}; see Fig. 9. A further increase in n_{5d} is obtained for the W compounds, although the R-Fe exchange decreases. This may suggest the existence of an optimum fraction of ~ 0.60 between the n_{5d} population and the number of conduction electrons at the R site, in order to promote the strongest R-Fe exchange in the $R\mathrm{Fe}_{12-x}\mathrm{T}_x$ compounds. The two experimental data for $R\mathrm{Fe}_{10.8}\mathrm{Re}_{1.2}$ compounds, with R=Tb and Ho (see Table IV) support the trend revealed in Fig. 9, and one may predict that a further decrease of n_{RFe} will occur with increasing n_{5d} when advancing through the $5d$ series to higher atomic numbers, such as T=Ir, Pt, and Au.

ACKNOWLEDGMENTS

This work was partially supported under CICYT MAT99/1142 grant and the Spanish-Romanian Bilateral Scientific Cooperation Program. N. P. gratefully acknowledges a fellowship granted by the Ministry of Education and Culture of Spain, as well as fruitful discussions with Dr. E. Palacios and Dr. D. P. Lazar. The authors acknowledge the critical reading of the manuscript by Dr. J. Chaboy.

*Also at National Institute of Materials Physics, PO-Box MG-07, Bucharest, Romania.

[1] K.H.J. Buschow, Rep. Prog. Phys. **54**, 1123 (1991).
[2] J.M.D. Coey and H.-S. Li, in *Handbook of Magnetic Materials*, edited by K. H. J. Buschow (Elsevier, Amsterdam, 1991), Vol. 6, p. 1.
[3] C. Piquer, M. Artigas, J. Rubín, and J. Bartolomé, J. Phys.: Condens. Matter **10**, 11 055 (1998).
[4] C. Piquer, E. Palacios, M. Artigas, J. Bartolomé, J. Rubín, J. Campo, and M. Hofmann, J. Phys.: Condens. Matter **12**, 2265 (2000).
[5] R. Vert, M. Bououdina, D. Fruchart, D. Gignoux, Y.M. Kalychak, and R.V. Skolozdra, J. Alloys Compd. **287**, 38 (1999).
[6] R. Vert, M. Bououdina, D. Fruchart, D. Gignoux, Y. Kalychak, B. Ouladdiaf, and R.V. Skolozdra, J. Alloys Compd. **285**, 56 (1999).
[7] B.P. Hu, K.Y. Wang, Y.Z. Wang, Z.X. Wang, Q.W. Yan, P.L. Zhang, and X.D. Sun, Phys. Rev. B **51**, 2905 (1995).
[8] K.Y. Wang, Y.Z. Wang, B.P. Hu, W.Y. Lai, and Z.X. Wang, J. Phys.: Condens. Matter **7**, 5365 (1995).
[9] J. Hu, Y. Wang, K. Wang, B.P. Hu, and Z. Wang, J. Alloys Compd. **288**, 57 (1999).
[10] R. Vert, D. Fruchart, D. Gignoux, and R.V. Skolozdra, J. Phys.: Condens. Matter **11**, 2051 (1999).
[11] R. Vert, M. Bououdina, D. Fruchart, D. Gignoux, S. Girard, B. Ouladdiaf, Y. Kalychak, and R.V. Skolozdra, J. Alloys Compd. **296**, 293 (2000).
[12] J.L. Wang, N. Tang, E. Brück, R. Zhao, F.M. Yang, and F.R. de Boer, J. Appl. Phys. **81**, 5131 (1997).
[13] A. Müller, J. Appl. Phys. **64**, 249 (1988).
[14] H. Sun, M. Akayama, K. Tatami, and H. Fuji, Physica B **183**, 33 (1993).
[15] M. Anagnostou, E. Devlin, V. Psycharis, A. Kostikas, and D. Niarchos, J. Magn. Magn. Mater. **131**, 157 (1994).

[16] B.P. Hu, H.S. Li, J.P. Gavigan, and J.M.D. Coey, J. Phys.: Condens. Matter **1**, 755 (1989).
[17] R. Coehoorn, Phys. Rev. B **41**, 11 790 (1990).
[18] D. Givord and D. Courtois, J. Magn. Magn. Mater. **196-197**, 684 (1999).
[19] Juan Rodriguez-Carvajal, *The XV-th Congr. Int. Union of Crystallography, Proceedings of the Satellite Meet. on Powder Diffraction, Toulouse, France* (1990), p. 127.
[20] A. Hérpin. *Théorie du Magnétisme* (Presses Universitaires de France, Paris, 1968).
[21] S.U. Jen and S.A. Chang, J. Appl. Phys. **73**, 6402 (1993).
[22] K.D. Durst and H. Kronmüller, J. Magn. Magn. Mater. **59**, 86 (1986).
[23] C.P. Yang, Y.Z. Wang, B.P. Hu, J.L. Wang, Z.X. Wang, Z.L. Jiang, C.L. Ma, and J. Zhu, J. Alloys Compd. **290**, 144 (1999).
[24] P.A. Algarabel, M.R. Ibarra, J. Bartolomé, L.M. García, and M.D. Kuz'min, J. Phys.: Condens. Matter **6**, 10 551 (1994).
[25] M.D. Kuz'min, J. Appl. Phys. **88**, 7217 (2000).
[26] K.H.J. Buschow, in *Ferromagnetic Materials*, edited by E.P. Wohlfarth and K.H.J. Buschow (Elsevier, Amsterdam, 1988), Vol. 4, p. 44.
[27] J.F. Herbst, Rev. Mod. Phys. **63**, 819 (1991).
[28] N.H. Duc, T.D. Hien, D. Givord, J.J.M. Franse, and F.R. de Boer, J. Magn. Magn. Mater. **124**, 305 (1993).
[29] E. Belorizky, M.A. Fremy, J.P. Gavigan, and H.S.Li D. Givord, J. Appl. Phys. **61**, 3971 (1987).
[30] M. Jurczyk, J. Magn. Magn. Mater. **89**, L5 (1990).
[31] H.S. Li, Y.P. Li, and J.M.D. Coey, J. Phys.: Condens. Matter **3**, 7277 (1991).
[32] E. Tomey. Ph.D. thesis, Université Joseph Fourier. Grenoble, 1994.
[33] M.S.S. Brooks and B. Johansson, in *Handbook of Magnetic Materials*, edited by K.H.J. Buschow (Elsevier, Amsterdam, 1993), Vol. 7, p. 139.
[34] E. Belorizky, J.P. Gavigan, D. Givord, and H.S. Li, Europhys. Lett. **5**, 349 (1988).
[35] L. Gelato, J. Appl. Crystallogr. **14**, 151 (1981).
[36] A.J. Freeman and J.P. Desclaux, J. Magn. Magn. Mater. **12**, 11 (1979).
[37] M.S.S. Brooks, O. Eriksson, and B. Johansson, J. Phys.: Condens. Matter **1**, 5861 (1989).